1 Compartmental models

Dr. I.H.M. van Stokkum

1.1 Introduction

Compartmental systems [1],[2] consist of a finite number of subsystems, called compartments, which exchange with each other and with the environment, so that the concentration of material within each compartment can be described by a first-order differential equation. Compartmental models are intensively used to describe pharmacokinetics (http://en.wikipedia.org/wiki/Pharmacokinetics), but also in epidemiology (wiki/Compartmental_models_in_epidemiology), chemical kinetics (wiki/ Chemical_kinetics and wiki/First_order_reaction and wiki/Reaction_rates), medical physics (e.g. wiki/ Fluorescein_angiography and wiki/Angiogram) and biophysics.

1.2 Mathematical model

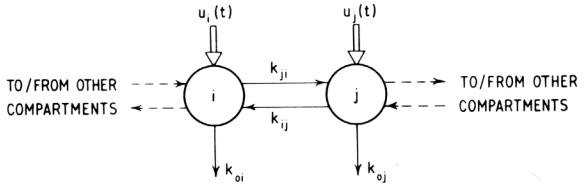

Figure 1.1 Two compartments of an LTI compartmental model. The k's are rate constants, so that flow rates are $k_{ij}x_j$, etc. The inputs $u_i(t)$ are flow rates

First, with a single compartment and input $i(t)$ the differential equation for the concentration, $\frac{d}{dt}c(t) = -k \cdot c(t) + i(t)$ has the solution $c(t,k) = \int_{-\infty}^{t} \exp(-k(t-s))i(s)ds = \exp(-kt) \oplus i(t)$ where $\oplus$ indicates convolution (see also the lecture notes of the Project Systems Modelling). With initial condition $c(0)$ we can put $i(s) = c(0)\delta(s)$ and find $c(t,k) = c(0)\exp(-kt)$. Now for multiple compartments, the general form of the linear differential equations describing a *p*-compartmental system is:

$$\frac{d}{dt}c_i(t) = \sum_{\substack{j=1 \\ j\neq i}}^{p} k_{ij}c_j(t) - \sum_{\substack{j=1 \\ j\neq i}}^{p} k_{ji}c_i(t) - k_{0i}c_i(t) + u_i(t) \qquad (1)$$

where $k_{ij}c_j(t)$ represents the flow to compartment *i* from compartment *j*, thus the first summation describes all input to compartment *i* from all other compartments. The k_{ij} are called the rate constants. Analogously, $k_{ji}c_i(t)$ represents the flow to compartment *j* from compartment *i*, thus the second summation describes all output from compartment *i* to all other compartments. Subscript 0 denotes the environment, and $k_{0i}c_i(t)$ is the flow from compartment *i* to the environment.

When an experimentalist is studying a complex system, the goal of the experiment is to arrive at a simplified description of the system and to estimate the essential physicochemical parameters (the rate constants from Eq. 1, and possible amplitude parameters, or delay parameters, etc.) with the help of a parameterized model. Most often such a model consists of a kinetic scheme containing transitions between states, which is a compartmental model. Taking into account the measurement conditions requires introduction of the instrument response function (IRF). In case the concentrations are described by linear differential equations we are dealing with first-

order kinetics. This can be considered a Linear Time Invariant (LTI) system with the IRF as input (the $u_i(t)$ from Eq. 1), and the vector of all compartments $c(t) = [c_1(t) \ldots c_p(t)]^T$ as output. The solution of a system of linear differential equations is given by a sum of exponential decays. Because it is an LTI system, the exponential decays have to be convolved with the IRF. The rate constants k_{ij} constitute the off-diagonal elements of the transfer matrix K. The diagonal elements of K contain the total decay rates of each compartment:

$$k_{ii} = -\sum_{\substack{j=1 \\ j \neq i}}^{p} k_{ji} - k_{0i} \tag{2}$$

Thus, the linear p-compartmental model is summarized by the system of differential equations:

$$\frac{d}{dt} c(t) = Kc(t) + u(t) \tag{3}$$

where the input to the system is described by a vector $u(t) = \left[u_1(t) \ldots u_p(t) \right]^T$.

Eq. 3 can be solved analytically, which is important for both insight into the problem and for computational speed. We assume that all eigenvalues of the transfer matrix K are different, and that c(-∞)= 0. The solution of Eq. 3 is then given by

$$c(t) = \int_{-\infty}^{t} \exp(K(t-s))u(s)ds = e^{Kt} \oplus u(t) \tag{4}$$

where $\oplus$ indicates convolution. This can be checked by differentiation of Eq. 4, which will give two contributions, and usage of the fundamental theorem of calculus $d\{\int_a^t f(s)ds\}/dt = f(s)\big|_{s=t}$ with $f(t - s) = \exp(K(t-s))u(s)$

$$dc(t)/dt = d\{\int_{-\infty}^{t} f(t-s)ds\}/dt = f(t-s)\big|_{s=t} + \int_{-\infty}^{t} \{df(t-s)/dt\}ds$$

Differentiation of $\exp(Kt) = \sum_{n=0}^{\infty} (Kt)^n / n!$ and usage of the chain rule results in $d\exp(Kt)/\mathrm{d}t = K\exp(Kt)$.

For a diagonal K-matrix $K = diag(-k_{01}, \ldots, -k_{0p})$, with all inputs equal to $i(t)$, the solution is given by (abbreviating $k_l = k_{0l}$)

$$c_l^I(t, k_l) = \int_{-\infty}^{t} \exp(-k_l(t-s))i(s)ds = \exp(-k_l t) \oplus i(t) \tag{5}$$

The superscript I indicates that this is Model I which is comprised of independently decaying compartments, and also is called the parallel model. When the IRF width is negligible the model reads $c_l^I(t) = c_l(0)\exp(-k_l t)$ with decay rate parameter k_l and amplitude parameter $c_l(0)$.

For the evaluation of the exponential of a non-diagonal K matrix we use the eigenvector-eigenvalue decomposition $K = U\Lambda U^{-1}$, with $\Lambda = diag(-k_1, \ldots, -k_p)$ the diagonal matrix containing the eigenvalues of K, and U the matrix with as columns the eigenvectors (check: $KU = U\Lambda U^{-1}U = U\Lambda$, thus each eigenvector is scaled by its eigenvalue). Thus we have $e^{Kt} = Ue^{\Lambda t}U^{-1}$ (since $\exp(Kt) = \sum_{n=0}^{\infty} (Kt)^n / n!$ and $K^n = U\Lambda U^{-1} \ldots U\Lambda U^{-1} = U\Lambda^n U^{-1}$ thus $\sum_{n=0}^{\infty} (Kt)^n / n! = U(\sum_{n=0}^{\infty} (\Lambda t)^n / n!)U^{-1} = U\exp(\Lambda t)U^{-1}$) and

$$e^{Kt} \oplus u(t) = Udiag(U^{-1}x)\begin{bmatrix} e^{-k_1 t} \oplus i(t) \\ ... \\ e^{-k_p t} \oplus i(t) \end{bmatrix} = Udiag(U^{-1}x)\begin{bmatrix} c_1^I(t) \\ ... \\ c_p^I(t) \end{bmatrix} \quad (6)$$

where $u(t) = i(t)x$ and $x = (x_1 \ ... \ x_p)^T$ is a vector that describes the amount of excitation of each compartment. Thus the solution of the general compartmental model is a linear combination of the c_j^I. **The concentration of each compartment is a linear combination of at most *p* exponential decays** (convolved with the instrument response function).

An example of a pharmacokinetic model is shown in Figure 1.2. It is left as an exercise for the reader to write down the transfer matrix K of this model. In pharmacokinetics also more complicated compartmental models are used, incorporating nonlinear differential equations, e.g. Michaelis-Menten kinetics. This is beyond the scope of this introductory text.

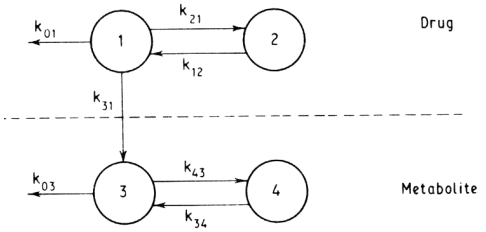

Figure 1.2 Typical two-compartment drug, two-compartment metabolite model.

1.3 The unbranched, unidirectional model

Apart from a model with independent decays (1 | 2 | … | *p*), the simplest kinetic scheme is the unbranched, unidirectional model (1 →2→…→*p*). These models are also termed parallel and sequential, and correspond to the generalization of the models I and II of section 6.6. In the sequential model back-reactions are ignored on the assumption that the energy losses are large enough that the reverse reaction rates are negligible. Note the assumption that there are no losses in the chain 1 →2→…→*p* . The compartmental model can be solved to yield [3]:

$$c_l(t) = \sum_{j=1}^{l} b_{jl} \exp(-k_j t) \oplus i(t) \quad (7)$$

where k_j is the decay rate of compartment *j* and the amplitudes b_{jl} of the (convolved) exponential decays are defined as $b_{11} = 1$ and for $j \le l$:

$$b_{jl} = \prod_{m=1}^{l-1} k_m \Big/ \prod_{\substack{n=1 \\ n \neq j}}^{l} (k_n - k_j) \quad (8)$$

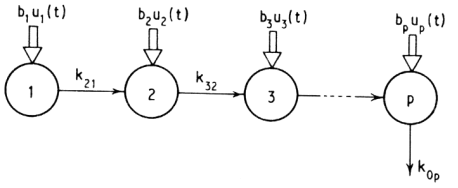

Figure 1.3 Catenary model with unidirectional exchange from the final compartment only. When $b_2 = \ldots = b_p = 0$ *it is a sequential model, otherwise a superposition of sequential models of different lengths.*

The K matrix now is of triangular form, and therefore the eigenvalues are on the diagonal. Take e.g. a two compartment sequential model where $K = \begin{bmatrix} -k_{21} & 0 \\ k_{21} & -k_{22} \end{bmatrix}$ and the eigenvalues are found from $Kx = \lambda x$, which requires $\det(K - \lambda I) = 0$ and thus $(-k_{21} - \lambda)(-k_{22} - \lambda) = 0$ which results in the two eigenvalues $-k_{21}$ and $-k_{22}$.

1.4 Closed systems

In a closed system no compartment excretes material to the environment. All closed systems have a zero eigenvalue. This zero eigenvalue corresponds to a constant term, the sum of all concentrations is constant:

$$\sum_{j=1}^{p} c_j(t) = c_{tot} \tag{9}$$

Thus a closed p-compartment system can be described by p-1 coupled ODE's plus equation (9).

1.5 Detailed balance

When two compartments *i* and *j* are at equilibrium, we have

$$k_{ij} c_j(t) = k_{ji} c_i(t) \tag{10}$$

and we can compute the Gibbs free energy difference between compartments *i* and *j* as

$$\Delta G_{ij} = k_B T \ln(k_{ji} / k_{ij}) \tag{11}$$

For a closed system at equilibrium the sum of the Gibbs free energy differences of a cycle equals zero. Thus e.g. with three compartments the product of the clockwise rate constants $1 \to 2 \to 3 \to 1$ is equal to the product of the counterclockwise rate constants $1 \leftarrow 2 \leftarrow 3 \leftarrow 1$:

$$k_{21} k_{32} k_{13} = k_{12} k_{31} k_{23} \tag{12}$$

This is called a detailed balance condition. Check that in this cycle the sum of the Gibbs free energy differences $\Delta G_{12} + \Delta G_{23} + \Delta G_{31}$ indeed equals zero when Eq.12 is used.

The dynamics of a closed system with three compartments that obeys the detailed balance condition will thus be described by the two negative eigenvalues of the K matrix that describe the approach to equilibrium with exponential decays, and a zero eigenvalue that describes the equilibrium. This will be studied further in the exercises.

1.6 Application to ocular fluorescein angiograms

A method has been proposed for estimating the choroidal blood flow parameters from fluorescein angiograms using simple compartmental models [5].

1.6.1 Introduction

The important contribution of the choroidal circulation to the nourishment of the outer retina and of the optic nerve head is a well-established fact. Its role in the pathogenesis of retinal disorders, or in potentially ischemic ocular conditions like glaucoma, has been postulated for a long time but is still an object of controversy. One of the reasons for this is the lack of a clinically acceptable technique for parameterizing choroidal blood flow. Since the advent of fluorescein angiography, it has been possible to visualize certain aspects of the retinal and choroidal circulations. The routine interpretation of

angiograms is still subjective and purely qualitative, but a substantial number of studies aimed at some form of quantification of retinal blood flow in vivo. This is not the case, however, for the choroidal circulation. Some attempts have been made to derive hemodynamic parameters from fluorescence-intensity curves obtained from angiographic sequences [4]. These attempts, highly computation-intensive, have been made possible by the popularization of image-processing facilities. That approach to the analysis of angiographic fluorescence-intensity curves, was based on a simple model of the choroidal filling. It was a variant of the dye-dilution curve analysis, assuming the entrance of the dye in the ocular vessels to be a step function, and the choroidal vasculature to behave like a single compartment. The purpose of introducing a second compartment [5] is to refine the approach by taking into account the conditions of ocular delivery of the dye, and to estimate the choroidal perfusion rate from routine clinical angiograms.

1.6.2 Materials and methods

Experimental

The data to be analysed have been extracted from routine clinical angiograms recorded on black-and-white negative films. The procedure for obtaining such angiograms is the following: after pharmaceutical dilation of the pupil and cannulation of a peripheral vein (usually the antecubital) the patient is seated in front of a fundus camera which incorporates a coaxial flash tube, a timer and an adequate set of filters. The fluorescent dye (in this case 3 ml of 25% sodium fluorescein) is then injected in the vein canula as fast as possible and at the same time, the timer of the camera is started. The time necessary for the dye to reach the eye through the systemic venous circulation, right heart, pulmonary circulation, left heart, and systemic arterial tree ("arm-retina" time) is 8-12 seconds. Six seconds after the injection, i.e. before the dye has reached the eye, photographs start being taken at the maximum rate of flash delivery (recharge), which is of the order of 0.75 to 1.0 second, depending on the camera. Photographs are taken at that rate until the end of the film. As some of the first frames of the film are used for recording patient data, white light and red-free light photographs of the fundus, approximately twenty frames are recorded per angiogram. The camera incorporates non-overlapping filters, positioned in front of the flash tube and of the film, ensuring that during angiography only the light emitted by the dye is recorded on the film. Thus, the first frames in the sequence (before arrival of the dye) are unexposed and the last frames, after the dye has penetrated all vessels, are nearly identical. Each frame is time-stamped by the camera. In routine clinical practice, paper prints made from the negatives are assessed by eye. For the present study, the central part of each negative (corresponding to an area approximately $25^{o} \times 25^{o}$ in the fundus) was digitized as an 8-bit 256 ×256 pixel image, using a black-and-white real-time frame grabber (Synaps-MAPP, Les Ulis, France) in a PC-AT type computer. A limited number of succesive frames (between 10 and 21) were digitized from each angiogram, starting a few seconds before arrival of the dye and, - whenever possible, extending a few seconds after the emitted intensity had reached its maximum value. Intensity build-up curves were extracted for each pixel over the whole sequence of digitized frames. The frames of each sequence were aligned manually relative to a reference frame from the middle of the sequence. In a few cases the alignment was improved with the help of an image processing algorithm which matched local regions of interest in successive images [6]. From these matches the optimal geometric transformation is found.

Theoretical

The simple model used in the preliminary studies [4] describes the concentration of fluorescein *c(t)* in a given site of the fundus by a first order differential equation. The differential equation of the one compartment model is

$$\frac{d}{dt}c_1^I(t) = -k_1 c_1^I(t) + i(t) \tag{13}$$

where k_1 is a rate constant (reciprocal of time constant) describing the rate of filling with fluorescein and *i(t)* is the speed of delivery of dye by the arteries to the fundus site per unit volume. The subscript 1 indicates compartment 1, whereas the superscript I indicates the simple exponential decay of this one-compartment model. With zero initial conditions and *i(t)* a step input, the solution of Eq.13 is given by (with $i(s) = c_{1,\infty}k_1$ if s positive, and else zero)

$$c_1^I(t) = \int_{-\infty}^{t} \exp(-k_1(t-s))i(s)ds = \int_{0}^{t} \exp(-k_1(t-s))(c_{1,\infty}k_1)ds = c_{1,\infty}(1-e^{-k_1 t}) \tag{14}$$

where $c_{1,\infty}$ is the steady state concentration resulting from the step input.

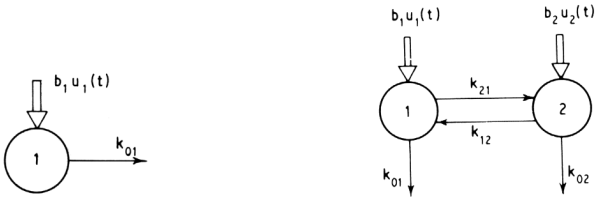

Figure 1.4 One-compartment model (left); general two-compartment model (right).

The next simplest model describes the concentration of fluorescein in a given site of the fundus with two coupled first order differential equations. Thereby compartment **2** represents the systemic circulation from the injection site to the arteries which supplies the ocular compartment **1**. The differential equations of the two-compartment model are

$$\begin{aligned} \frac{d}{dt}c_2^{II}(t) &= -k_2 c_2^{II}(t) + i(t) \\ \frac{d}{dt}c_1^{II}(t) &= -k_1 c_1^{II}(t) + k_{12} c_2^{II}(t) \end{aligned} \tag{15}$$

k_2 is a rate constant describing the rate of filling with fluorescein of compartment **2**. $k_{12}c_2^{II}(t)$ is the speed of delivery of dye by the arteries to the fundus site per unit volume. *i(t)* represents injection of dye in a peripheral vein. For this scheme the transfer matrix *K* is of upper triangular form:

$$K_{II} = \begin{bmatrix} -k_1 & k_{12} \\ 0 & -k_2 \end{bmatrix} \tag{16}$$

With zero initial conditions and *i(t)* a step input we have the solution

$$\begin{aligned} c_2^{II}(t) &= c_{2,\infty}(1-e^{-k_2 t}) \\ c_1^{II}(t) &= c_{1,\infty}(1-\tfrac{k_1}{k_1-k_2}e^{-k_2 t} + \tfrac{k_2}{k_1-k_2}e^{-k_1 t}) \end{aligned} \tag{17}$$

$c_{1,\infty}$,and $c_{2,\infty}$,are the steady state concentrations resulting from the step input, $c_{2,\infty}$, = $c_{1,\infty}k_1/k_{12}$. In case $k_1 = k_2$ we find $c_1^{II}(t) = c_{1,\infty}(1-e^{-k_1 t} - k_1 t e^{-k_1 t})$. (18)

Note that the eigenvalues of the *K* matrix are the diagonal elements ($-k_1$,$-k_2$), and that the solution consists of linear combinations of exponential decays with these rate constants.

In routine angiography the fluorescence intensity is measured as a function of fundus position at *n* sequential time instants, typically *n* = 20. We assume this intensity to be proportional to $c_1(t)$, the fluorescein concentration in a fundus site. We also assume this intensity to be proportional to the density of the film *f(t)*, which is the quantity actually measured. These assumptions are valid within given ranges of dye concentration and film exposure, respectively.
Another assumption in the design of the models is that the fluorescence emitted from fundus sites with no dominant retinal features (macula, retinal vessels) originates essentially from the choriocapillaris level. Alternative sources of fluorescence might be (a) dye in the more superficial (retinal) microcirculation, and (b) in the deeper (large choroidal vessel) layers. This point is discussed further on. Because the number of time points is small, we cannot estimate the systemic dynamics parameter k_2 from each fundus site separately. We therefore decided to link k_2 across the fundus. In practice a grid of m fundus sites, typically m = 64, was used.
The one-compartment model function for the film density *f(t)* which is assumed to be proportional to dye concentration in a fundus site contains three parameters which need to be estimated. Parameter *d* represents the steady state level of the film density, t_0 represents the delay time from the moment of injection. Because a rate constant is by definition positive, we fitted its logarithm. Thus we arrived at the model function

$$f^{I}(t) = d(1 - e^{-k_1 t}) \text{ with } t = t_j - t_0 > 0 \text{ and } \quad j = 1, n\,. \tag{19}$$

The parameterization of Eq.17 requires the extra systemic rate parameter k_2 (which we again forced to be positive by fitting its logarithm) which gives the two-compartment model function to be fitted.

$$\begin{aligned} f^{II}(t) &= d(1 - \tfrac{k_1}{k_1 - k_2} e^{-k_2 t} + \tfrac{k_2}{k_1 - k_2} e^{-k_1 t}) \\ t &= t_j - t_0 > 0; j = 1, n \end{aligned} \tag{20}$$

The parameter estimation procedures were implemented in Fortran 77 using mathematical and statistical routines. To speed up the nonlinear least squares (NLLS) fitting of the two-compartment model we eliminated the linear parameters with help of the *variable projection* method. Typical computation times on a 1995 workstation for an 8x8 grid of fundus sites were 20 and 200 seconds for, respectively, one- and two-compartment fitting.

1.6.3 Results

We will present results from one patient (*lgm*) in detail, whereas the results from a population study of 48 patients will be summarized. These patients suffered either from glaucoma (primary open angle or normal pressure) or from diabetic retinopathy. The relation between the estimated parameters and the clinical status of these patients is beyond the scope of this paper and is still under investigation. In our preliminary study [4], each of the 256×256 density curves was analysed independently using Eq.19. If, however, the extra parameter (k_2) is to be introduced in the model, all the time-curves have to be fit simultaneously. Clearly, a simultaneous fit of all 256x256x2 +1 parameters is not feasible. Therefore k_2 is estimated from a regularly spaced 8x8 selection, and k_2 is fixed when fitting Eq.20 for all 256x256 density curves.
Thus we can estimate 256x256 parameters d, k_1, t_0 from a one-compartment model (Eq.19) and from a two-compartment model (Eq.20).

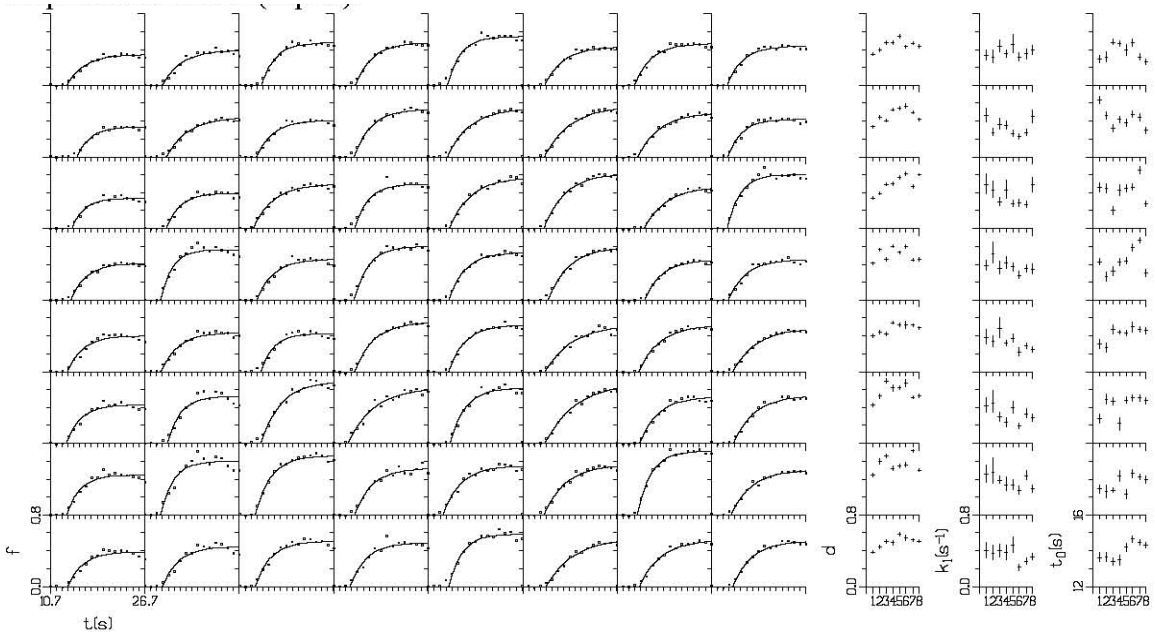

Figure 1.5 Overview of fit results of density curves (of n = 17 points) from patient lgm using the one-compartment model. Fitted curves are shown at the 8x8 fundus points. In the three rightmost columns, respectively, d, k1 and t_0 belonging to a row of fundus sites are drawn. The plusses indicate the estimates, with the vertical bar indicating the approximate standard error in the parameters $\pm\sigma_d$ etc.

In Figure 1.5 and Figure 1.6 we see the results of fits of data obtained from patient *lgm* at a grid of 8x8 distinct fundus sites (regularly distributed over the whole fundus area, as indicated by the squares in Figure 1.7 and Figure 1.8) with, respectively, the one- and two-compartment model. The improved alignment procedure was applied to these data. The global root-mean-square error σ (from the NLLS fit) decreases from 0.0320 to 0.0282 when the second compartment is added. When we define the relative improvement γ as $\gamma = (\sigma_I - \sigma_{II})/ \sigma_I$ this amounts to a 12% improvement of the fit. Comparing Figure 1.5 and Figure 1.6 the improvement gained with the two-compartment model is visible in the onset of the density curve in many fundus sites.
In the three rightmost columns, parameter estimates (respectively, d, k_1 and t_0) belonging to a row of fundus sites are drawn. The plusses indicate the NLLS estimates, with the vertical bar indicating the error in the parameters, $\pm\sigma_d$ etc.

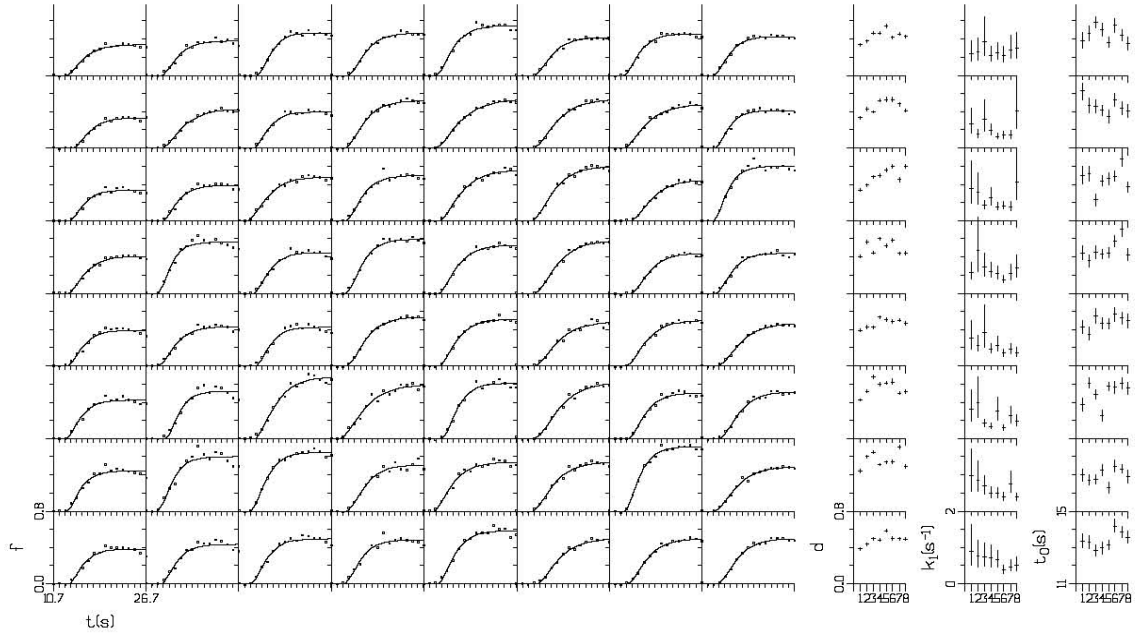

Figure 1.6 Overview of fit results of the same 8x8 density curves from patient lgm using the two-compartment model. Layout as in Figure 1.5.

Note that the differences between the k_1 and t_0 parameters of the one- and two-compartment model depend upon the extra parameter k_2. The uncertainty in the estimated parameters is small for the maximum density *d*, but large for the rate and appearance time parameters (tens of percents relative error), as it can be seen from the vertical bars in the first and the last two columns of Figure 1.5 of and Figure 1.6. Introduction of the second compartment rate parameter of course increases these uncertainties.

We compared the two models for analysis of the angiograms of the patients described in the beginning of this section. Of 48 angiograms studied we found a relative improvement of the goodness of fit $\gamma \geq 5\%$ in 26 cases when the second compartment is introduced. The maximum improvement found was 17%. In 11 cases $1\% \leq \gamma \leq 5\%$ and in 11 cases $0\% \leq \gamma \leq 1\%$.

The rate constant of the global compartment (systemic circulation), k_2, could be reliably determined in 37 cases. The ranged from 0.12 – 1.66 s^{-1}, 31 of them possessed values in the interval of 0.30 – 1.00 s^{-1}.

Figure 1.7 and Figure 1.8 depict grey scale maps of the parameters estimated for patient *lgm* using respectively, the one and two compartment models. The grey scale is designed with the convention that darker indicates “worse” circulation (i.e. lower maximal density, lower rate of perfusion and later appearance time) whereas lighter indicates “better” circulation. The squares indicate the grid of 8x8 fundus sites used with Figure 1.5 and Figure 1.6. E.g. the site row 7, column 7 corresponds to an artery, with a large value of *d*. The maximum density maps (Figure 1.3a and Figure 1.8a) are not very different from a late angiographic frame. In the rate maps (Figure 1.7b and Figure 1.8b) a lower perfusion rate is visible in the temporal half of the choriocapillaris.

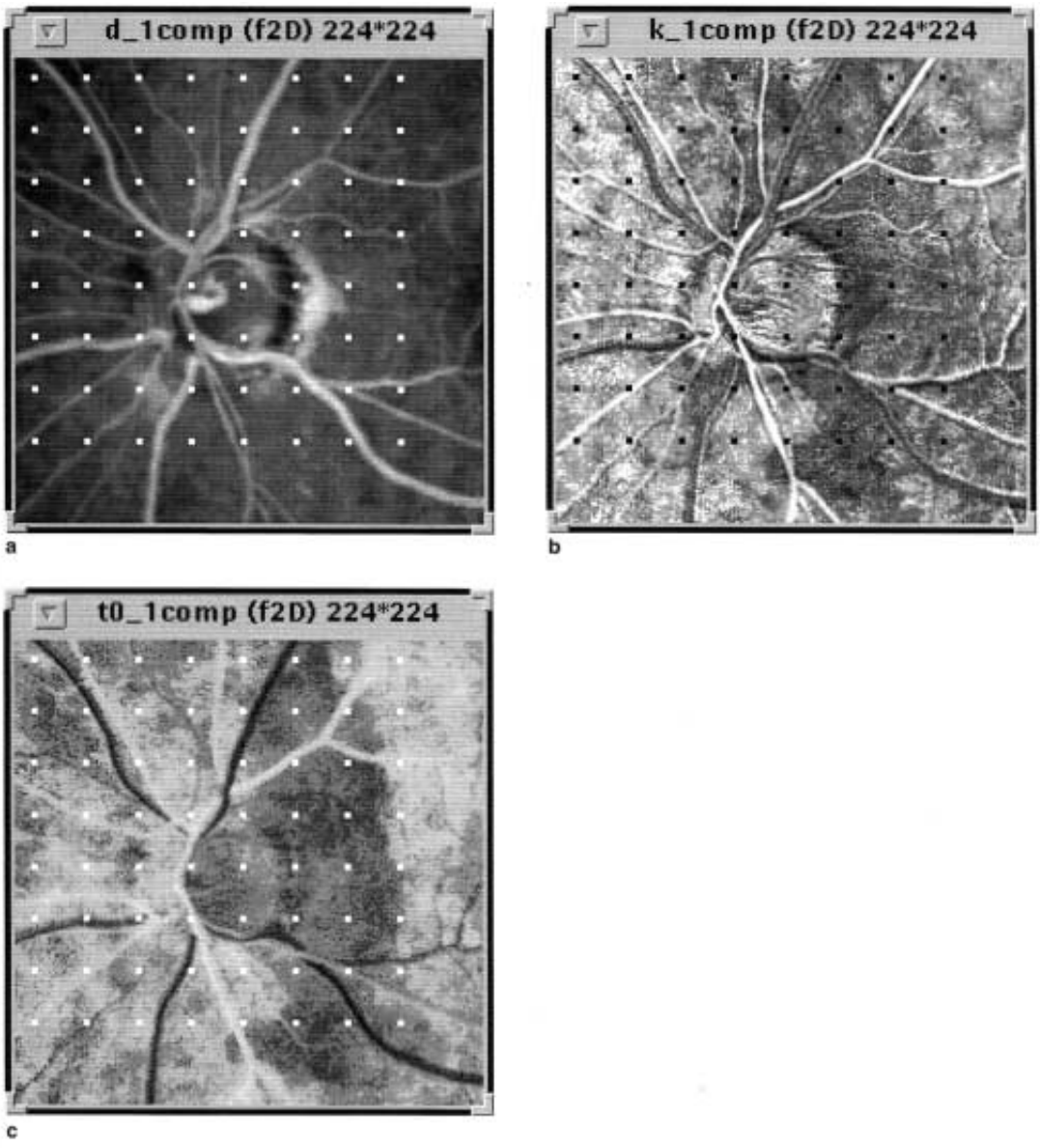

*Figure 1.7 Grey scale maps (224*224 pixels) of estimated parameters from patient* lgm *using the one compartment model. The squares indicate the positions of the 8x8 grid used in and. (a) Maximum density d. (b) Local perfusion rate* k_1. *(c) Delay time* t_0. *Extrema (respectively, black and white): (a) 0.278 and 0.905. (b) 0.118 and 0.572* s^{-1}. *(c) 16.36 and 12.54* s^{-1}.

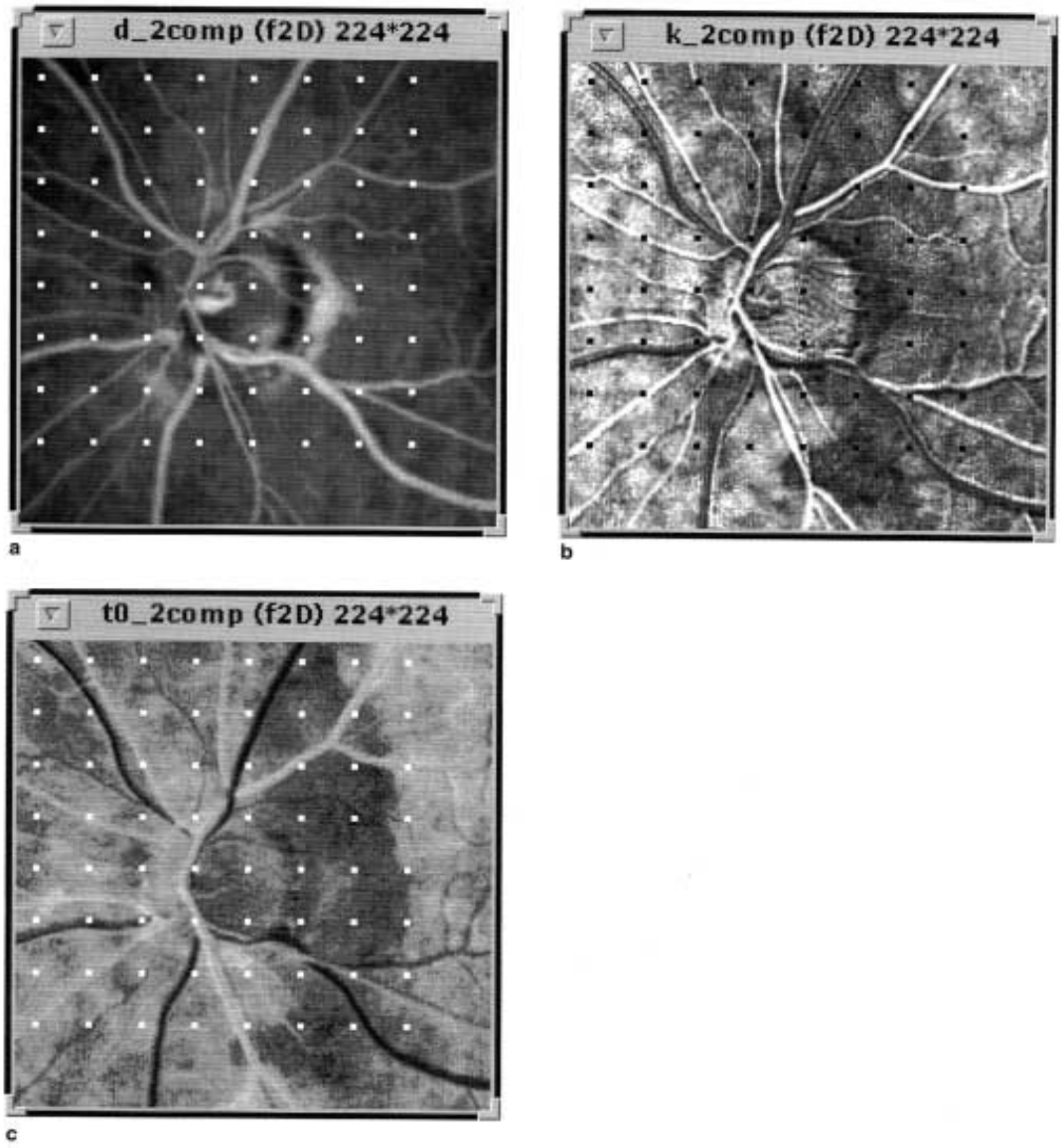

Figure 1.8 Grey scale maps of estimated parameters from patient lgm using the two-compartment model. Layout as in Extrema: (a) 0.278 and 0.905. (as in a) (b) 0.156 and 0.934 s^{-1}. (c) 15.43 and 11.61 s^{-1}. Note that the difference between these extrema is the same as in c.

Comparing the two maps, some differences can be seen. Figure 1.8b represents a larger dynamic range of k_1 and provides a better contrast than Figure 1.7b. With patient *lgm* the local rate k_1 varied between 0.29 – 0.92 s^{-1}, whereas the global rate k_2 was estimated to be about 0.64. Finally, the t_0 maps (Figure 1.7c and Figure 1.8c) show a highly delayed appearance in the territory temporal to the optic nerve head. Comparing the two maps, this delay appears to be closer to the t_0 of the veins in Figure 1.8c than in Figure 1.7c.

1.6.4 Discussion

The interpretation of fundus fluorescence build-up curves requires some assumption about the origin of the fluorescent light given the fact that a complex 3-dimensional angioarchitecture is projected on 2-dimensional angiographic frames.
In a normal fundus, one can roughly distinguish three circulatory layers. The (most superficial) retinal circulation is the most striking feature of the angiogram because of the high contrast and crisp detail of its vessels. It is evident that fluorescence recorded

over such vascular features originates predominantly from intravascular dye. The retinal microcirculation, however, has limited contribution to fundus fluorescence because of its small volume and since the blood-retina barrier precludes dye-leakage. This is supported by two types of angiographic evidence: In areas of delayed, masked or inexistent choroidal filling (e.g. with targeted dye delivery) smaller retinal vessels can be resolved but neither the actual capillary network nor any homogeneous capillary fluorescence are visible. A contrario, when there is a breakdown of the blood-retina barrier, the leakage of dye in the retinal tissue results in a strong fluorescent spot obscuring the deeper (choroidal) layers.

So, in the absence of such distinctive retinal features, the fluorescent light originates from the choriodal level. Absorption by hemoglobin and fluorescein (intravascular or extravasated) restricts the penetration depth of the exciter light to ca. 30 µm, limiting strongly the contribution of the large choroidal vessels to fundus fluorescence. Only in the presence of an exceptionally thin or atrophic choriocapillaris do these vessels become visible in the early angiographic frames.

The two-compartment model allows a separation of hemodynamic properties of systemic and choroidal circulation, thus giving a better basis for usage of this analysis. On the other hand, the quality of fit of the one-compartment model is already quite good (and), so this model is apt for not too demanding applications. A clear improvement in goodness of fit from using a two-compartment model is present in 26 ⁄48 cases, whereas a moderate improvement is found in 11⁄48 cases. It is natural that addition of the extra parameter, the rate constant of the second compartment, never causes deterioration of the NLLS fit. The success of the two-compartment model depends upon the quality of the data (signal to noise ratio) and namely upon

- the number of data points taken during the rising phase of the density curve
- the availability of data points before and after the rising phase.

With respect to the quality of the data, special efforts have been made towards correct alignment of the photographs, manually or automatically [6], in order to improve the fit of the density build-up curves since shifts of a few pixels across vessel edges cause large outliers.

It is remarkable that about one image per second is sufficient for fitting such a complicated model with rate constants of about 0.7 s^{-1}. It is to be expected that a higher temporal resolution will enable a more accurate estimation of the parameters. With a higher temporal resolution the cyclic variation that may be caused by the cardiac cycle might have to be incorporated into the model. This now could be a source of error in the data.

The grey scale maps of parameters (Figure 1.7 and Figure 1.8) present a concise summary of the angiographic sequence, which can be interpreted quantitatively. In particular, the information presented in the perfusion rate map (b and b) is very hard to extract by eye from an angiographic sequence, even with experienced examiners. When angiograms are interpreted subjectively, prominent features like retinal microaneurysms or choroidal watershed zones are immediately recognized and characterized by the examiner, but an assessment of the choroidal perfusion requires a very careful scrutiny of the whole sequence and an important amount of mental abstraction, if one wants to separate factors leading to the observed fluorescence patterns. Transient choroidal hypofluorescence, for instance, may be either due to late dye appearance, or to slow filling, or both. By separating the two phenomena, the method presented here reduces the number of images to be assessed to three (the three parameter maps instead of the whole angiographic sequence), facilitates the qualitative interpretation of the choroidal circulation, and permits to parameterize the choriocapillaris perfusion.

1.6.5 References

[1] D.H. Anderson, *Compartmental modeling and tracer kinetics.* Springer, Berlin, 1983.
[2] K. Godfrey, *Compartmental models and their application.* Academic Press, London, 1983.
[3] J.F. Nagle, L.A. Parodi, R.H. Lozier (1982) Procedure for testing kinetic models of the photocycle of bacteriorhodopsin. Biophys. J. 38, 161-174.
[4] Lambrou GN, Van den Berg TJTP, Greve EL (1989) Vascular plerometry of the choroid. An approach to the quantification of choroidal blood flow using computer-assisted processing of fluorescein angiograms. In: Lambrou GN, Greve, EL (eds) Ocular blood flow in glaucoma. Kugler & Ghedini, Amsterdam, pp. 287-294.
[5] Van Stokkum, I.H.M., Lambrou, G.N., Van den Berg, T.J.T.P. (1995) Hemodynamic parameter estimation from ocular fluorescein angiograms. *Graefe's Archive for Clinical and Experimental Ophthalmology* 233, 123-130.
[6] In den Haak MD, Spoelder HJW, Groen FCA (1992) Matching of images by using automatically selected landmarks. In: Dietz JLG (ed) Proceedings of Computer Science in the Netherlands 1992. Stichting Mathematisch Centrum, Amsterdam, pp. 27-40.

Question 3: compartmental model of a light harvesting antenna **(**30 points)

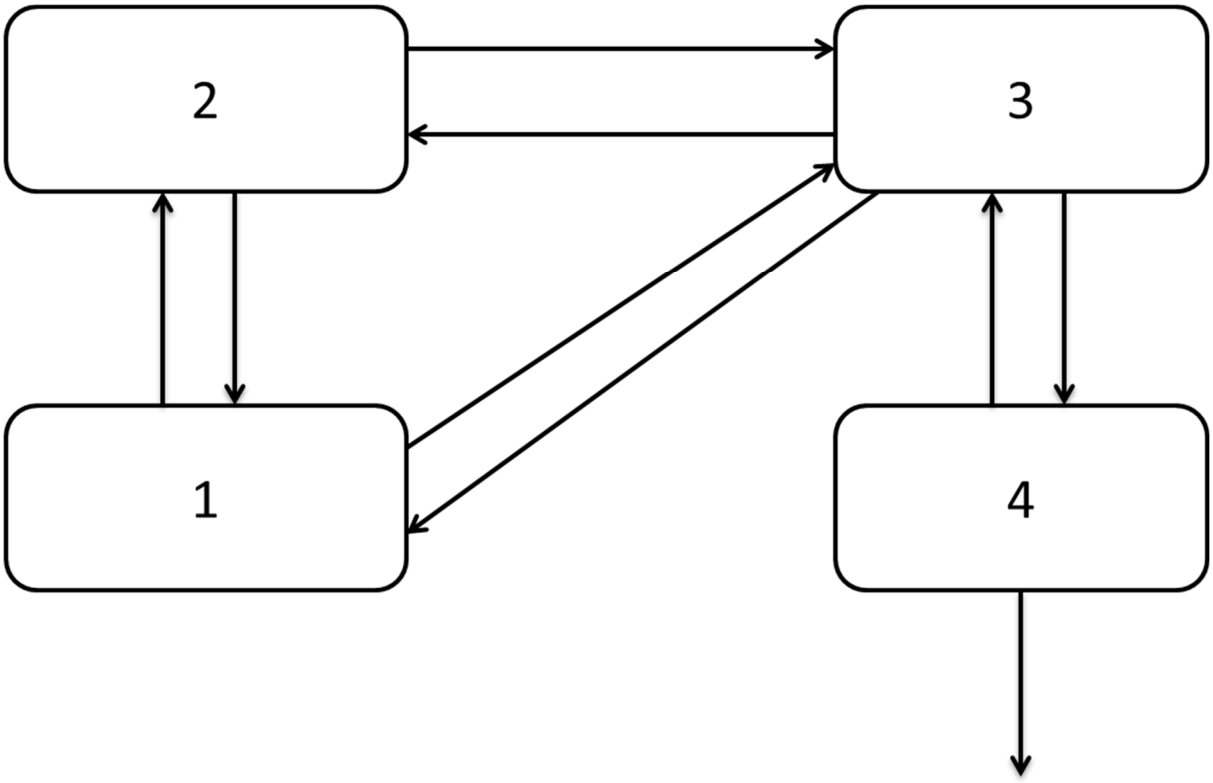

a. (6p) Add rate constant names k_{ij} describing the flow to and from all compartments.
Then write down the matrix/vector differential equation that describes the above compartment system, assuming that there is no external input, but only initial conditions $c_1(0) = c_2(0) = 1$, $c_3(0) = 0.75$ and $c_4(0) = 0$.

b. (4p) Write down the formal, analytical solution to the matrix equation from **a**, assuming that the initial condition is a vector **c(0)**.

How do the observed decay rates (reciprocals of the observed lifetimes) relate to this solution?
(2 lines)

c. (4p) Formulate the detailed balance condition for this compartment system. Assuming that the detailed balance condition holds, given the values $k_{31} = 1.2, k_{13} = 1.6, k_{12} = 40, k_{43} = 200, k_{34} = 50, k_{23} = 80, k_{32} = 60$, what is k_{21}?

d. (3p)What is the Gibbs free energy difference between compartments 1 and 3 (use $k_B T = 25$ meV) ?

e. (4p)Draw a Gibbs free energy level scheme for the four compartments, or describe this scheme in words.

f. (5p) Describe qualitatively what you observe in these two plots of this system. (3-5 lines)

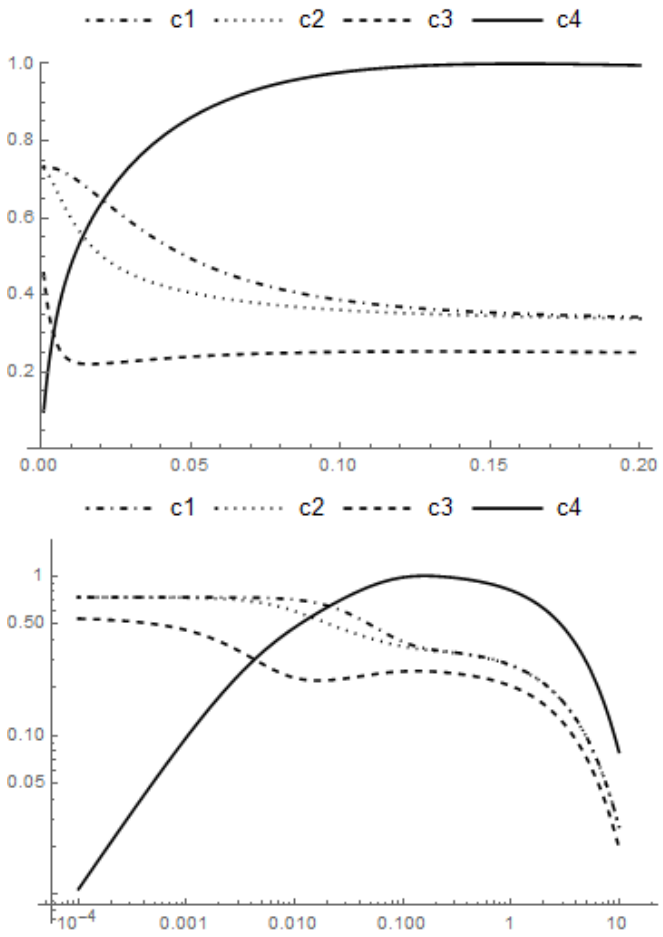

g. (4p) Estimate the decay rate k_{04} from the plots in f.